



## ORIGINAL ARTICLE

# Immobilization of bismuth oxychloride on cellulose nanocrystal for photocatalytic sulfonylation of arylacetylenic acids with sodium arylsulfonates under visible light



Xiaoxia Wang<sup>a,b</sup>, Xueting Li<sup>a</sup>, Baoqiang Tian<sup>a</sup>, He Xiao<sup>a</sup>, Wenwen Chen<sup>a,\*</sup>,  
Haishun Wu<sup>a</sup>, Jianfeng Jia<sup>a,\*</sup>

<sup>a</sup> Key Laboratory of Magnetic Molecules & Magnetic Information Materials Ministry of Education School of Chemical and Material, Science Shanxi Normal University, Taiyuan 030006, PR China

<sup>b</sup> Department of Chemistry, Changzhi University, Changzhi 046011, PR China

Received 17 November 2021; accepted 16 January 2022

Available online 28 January 2022

## KEYWORDS

Cellulose nanocrystal;  
Bismuth oxychloride;  
Photocatalyst;  
Sulfonylation reaction

**Abstract** As a promising semiconductor photocatalyst, BiOCl has been widely used in the field of environmental protection. However, due to its weak ability to absorb visible light, the application of BiOCl in other important photocatalytic fields has been significantly limited, such as organic synthesis. In this work, a facile method was used to prepare a highly efficient heterogeneous nanophotocatalyst BiOCl/cellulose nanocrystal (CNC). Subsequently, the BiOCl/CNC was verified by XPS, ESR, BET and other characterization methods. The results show that not only the strong interaction between BiOCl and CNC increases the visible light absorption intensity of the composite, but also the combination of BiOCl and CNC makes the specific area of the catalyst more than twofold. In addition, a large number of hydroxyl groups contained in CNC can be combined with the B—O bond in BiOCl through hydrogen bonds, forming abundant oxygen vacancies on BiOCl/CNC. Excitedly, these changes enable BiOCl/CNC to exhibit excellent photocatalytic performance and regeneration performance in the sulfonylation reaction of arylacetylene acid and sodium arylsulfinate, with a yield of up to 96%. This work represents a step towards a low-cost,

\* Corresponding author at: Key Laboratory of Magnetic Molecules & Magnetic Information Materials Ministry of Education School of Chemical and Material, Science Shanxi Normal University, Taiyuan 030006, PR China

E-mail addresses: chenww@sxnu.edu.cn (W. Chen), jiajf@dns.sxnu.edu.cn (J. Jia).

Peer review under responsibility of King Saud University.



environmentally friendly composite of cellulose and BiOCl, which will provide useful enlightenment for future exploration in related fields.

© 2022 The Author(s). Published by Elsevier B.V. on behalf of King Saud University. This is an open access article under the CC BY-NC-ND license (<http://creativecommons.org/licenses/by-nc-nd/4.0/>).

## 1. Introduction

Using photocatalyst to capture and convert solar energy for chemical fuel storage and industrial applications is a paramount way to achieve sustainable development of human society (Fava et al., 2016; Xu et al., 2017). As a classical two-dimensional semiconductor material, BiOCl not only has low cost, nontoxicity, morphological variation and convenient preparation, but also has high chemical stability and catalytic activity (Han, 2021). In addition, in the unique layered structure of BiOCl,  $[\text{Bi}_2\text{O}_2]^{2+}$  is connected with halogen atom layer through intermolecular force, and this unique structure can facilitate the generation of an internal self-built electric field between Cl atom layer and  $[\text{Bi}_2\text{O}_2]^{2+}$  layer, which will greatly promote the separation of electrons and holes and improve the photocatalytic performance (Hojamberdiev et al., 2020; Liu et al., 2021). Based on these advantages, BiOCl has captured extensive attention and has been widely studied in the field of environmental protection, including sewage treatment (Gao et al., 2018; Gao et al., 2020; Gao et al., 2021; Liu et al., 2021; Monga and Basu, 2021), degradation of organic dyes (Guerrero et al., 2014; Zhang et al., 2014; Zhang et al., 2020) and purification of polluted air (Wu et al., 2020). Regrettably, the application of BiOCl in other important visible light photocatalytic fields has been greatly limited, such as organic synthesis, which may be attributed to its difficulty to produce active electrons and holes to stimulate organic reactants under visible light as a wide band gap semiconductor (Han et al., 2019; Yang et al., 2021). In view of this, it is of great significance to develop a BiOCl-based photocatalyst that can be effectively used in organic synthesis and other important visible light catalysis fields.

As we all know, the BiOCl can be combined with a variety of matrices to form BiOCl/matrix composite materials, such as BiOCl/TCPP (Huang et al., 2021) and BiOCl/polyaniline (PANI) (Mansor et al., 2021), to achieve significant improvement of the spectral absorption range and photocatalytic efficiency. However, these matrix carriers are usually non-degradable and unsustainable, and may even introduce new toxins in the application. Another fact that cannot be ignored is that most matrices need to be produced through fossil energy and cannot fundamentally solve environmental problems. As a green, sustainable and renewable resource, cellulose not only has high hydrophilicity, permeability, transparency, physical and chemical resistance and thermal stability, but also can firmly fix the catalyst through its own large number of hydroxyl groups (Kamel and Khattab, 2021; Shi et al., 2021). In addition, the abundant hydroxyl contained in cellulose may interact with the low-energy Bi—O bonds in BiOCl through hydrogen bond to build a large number of oxygen vacancies on the surface of BiOCl, which is considered to be an important means to improve the photocatalytic activity of BiOCl (Li et al., 2018). Among a variety of cellulose, cellulose nanocrystal (CNC) deserves more attention because it not only contains a large number of hydroxyl groups, but also its specific surface area is nearly 100 times larger than that of other types of cellulose (Hamad, 2018; Ng et al., 2021), which makes it possible for CNC as matrix to significantly improve photocatalytic performance (Du et al., 2018; Elfeky et al., 2020; Tian et al., 2019; Zhan et al., 2018). Therefore, the preparation of composites with BiOCl by CNC is of great significance to improve the photocatalyst performance of BiOCl and expand its photocatalytic fields.

Sulfones have a broad spectrum of biological activities and are extensively used in the fields of chemistry, medicine, pesticide, material science (Llamas et al., 2006; Sulzer-Mosse et al., 2009; Yang et al., 2008; Zhu et al., 2008). At the same time, due to their ability to stabilize  $\alpha$ -carbanions and strong electron-withdrawing properties, sulfones

have been favored by synthetic chemists for so long. Arylacetylenic sulfones are an important derivative of sulfone, which has prominent applications in synthesis, e. g., as dienes in cycloadditions (Riddell and Tam, 2006; Zhao and Beaudry, 2014; Zhou et al., 2015), in the synthesis of disubstituted alkynes and in the alkynylation of diverse structures of biological interest (Meadows and Gervay-Hague, 2006; Todoroki et al., 2014). Due to the important application value of arylacetylenic sulfones, a variety of synthetic methods have been developed in recent years. However, the traditional synthesis methods of arylacetylenic sulfones encounter some limitations, such as harsh synthesis conditions, cumbersome synthesis process, the need of stoichiometric oxidants (Chen et al., 2017; Meesin et al., 2016; Wang et al., 2017; Zhong et al., 2020). Compared with traditional synthesis and electrocatalysis, photocatalysis utilizes light energy to stimulate electrons to initiate chemical reactions, which can realize the breaking and recombination of chemical bonds under mild conditions. Predictably, photocatalysis will be a more coveted method to synthesize arylacetylenic sulfones, but it has never been achieved so far.

Herein, CNC has abundant hydroxyl groups and high specific surface area, which plays an important role in increasing the active surface area and improving the performance of photocatalyst. In addition, the high physical and chemical stability of CNC also helps to improve the recycling capacity of the composites. As expected, BiOCl/CNC has demonstrated excellent photocatalytic performance and reusability in the sulfonylation reaction of aryl acetyl acid and sodium arylsulfinate, then, a series of control experiments have proposed the possibility photocatalytic reaction mechanism.

## 2. Experimental

### 2.1. Preparation of CNC

According to previously reported literature (Hu et al., 2017), CNC was prepared by acid hydrolysis of microcrystalline cellulose (MCC) as follows: MCC (10 g) was slowly added to a beaker containing 150 mL sulfuric acid of 64 wt% and stirred continuously. MCC was completely dispersed in water and heated at 45 °C until MCC was completely hydrolyzed. The resulting yellow solution was diluted 7-fold by ultrapure water, left standing and the upper clear solution was poured away. The remaining suspension was washed via centrifugation until it was no longer layered. The obtained sample was dialyzed against ultrapure water until neutral. Finally, the obtained CNC suspension was subjected to ultrasonic treatment at room temperature for 5–10 min and stored in cold storage for next experiments.

### 2.2. Fabrication of BiOCl/CNC nanocomposite

BiOCl/CNC nanocomposite was obtained by in situ synthesis at room temperature (rt). In this process, 1.0 mmol KCl was added into 20 mL CNC solution under magnetic stirring. 1.0 mmol of  $\text{Bi}(\text{NO}_3)_3 \cdot 5\text{H}_2\text{O}$  was completely dissolved in 5 mL ethylene glycol (EG) by ultrasonication. Then the suspension was dropwise in CNC solution and stirred at rt for 1 h. Subsequently, the deposit was collected and washed via

centrifugation and dried with vacuum drying at 60 °C for 8 h. Similarly, BiOCl was obtained by the same way except that the 1.0 mmol KCl was added into 20 mL ultrapure water instead of CNC solution.

### 2.3. Characterization and reactant preparation

The methods for characterization and organic reactant preparation are shown in [Supplementary Data](#).

## 3. Results and discussion

### 3.1. Characterization and study on the interaction between BiOCl and CNC in the photocatalyst

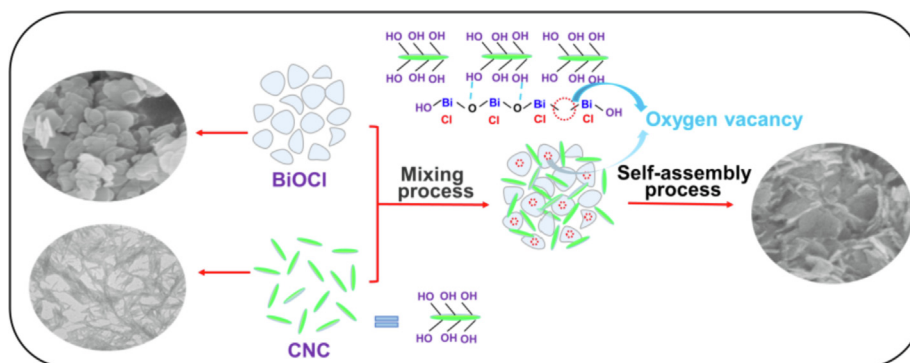
The possible growth mechanism of BiOCl/CNC was proposed as manifested in [Scheme 1](#). Nanorod-shaped nanocellulose and lamellar BiOCl self-assembled into three-dimensional BiOCl/CNC nanosheets. In the specific growth process,  $\text{Bi}^{3+}$  was preferentially strongly adsorbed onto the microporous structure of CNC due to a large number of hydroxyl groups in the molecular chain of CNC. In addition, hydrogen bonding and electron interaction can prevent the aggregation of  $\text{Bi}^{3+}$  and promote the formation of oxygen vacancies ([Tian et al., 2019](#); [Li et al., 2018](#)), and then three-dimensional BiOCl/CNC nanosheets were formed through self-assembly, thereby improving its photocatalytic performance.

X-ray diffractometer (XRD) pattern of BiOCl/CNC ([Fig. S1a](#)) is similar to BiOCl, which is indicative of the lattice structure of BiOCl will not be changed by the combination with CNC. Compared with pure BiOCl, there are significant changes that the stronger (1 1 0) diffraction peak corresponding to  $2\theta = 32.5^\circ$ , which shows that the prepared BiOCl/CNC presents high percentage of exposed (1 1 0) facets. Previous studies have demonstrated that the increased exposure of the (1 1 0) facet in the BiOCl structure can improve the separation efficiency of photogenerated carriers, which is beneficial to enhance the photocatalytic activity of BiOCl/CNC ([Wang et al., 2019](#)). As described in [Fig. S1b](#), the functional groups of BiOCl and BiOCl/CNC and their interactions were analyzed by FT-IR. The absorbance bands at  $\sim 3200\text{--}3500\text{ cm}^{-1}$ ,  $2850\text{--}3000\text{ cm}^{-1}$  and  $1059\text{--}1162\text{ cm}^{-1}$  can be assigned to hydroxyl groups, C—H stretching and C—O—C stretching in CNC, respectively. The peak at  $524\text{ cm}^{-1}$  may be indexed to Bi—O bond vibration ([Gao et al., 2015](#)) and the peak at

$1419\text{ cm}^{-1}$  is ascribed to Bi—O bond stretching vibration ([Soleimani et al., 2017](#)). Combined with XRD results, it can be concluded that BiOCl is successfully loaded onto CNC and there is a strong interaction between the two interfaces.

Subsequently, scanning electron microscope (SEM) and transmission electron microscopy (TEM) were used to analyze the morphology and microstructure of BiOCl and BiOCl/CNC. As described in [Fig. 1a](#), the surface of BiOCl nanosheets is smooth and stacked with each other without the addition of CNC. Interestingly, its morphology becomes three-dimensional cross-type thin nanosheets with the addition of CNC ([Fig. 1b, 1c](#)), which is attributed to the dried CNC assemble into a hierarchical structure. The HRTEM images shows two types lattice stripes with lattice spacings of 0.275 and 0.344 nm, matching (1 1 0) and (1 0 1) facets of BiOCl, respectively ([Fig. 1d](#)) ([Jia et al., 2021](#); [Wu et al., 2021](#)), which matched with the XRD. And the element mapping of BiOCl/CNC composite further scientific evidence for the uniform distribution of Bi, O and Cl elements on the material ([Fig. 1e–1h](#)). Thermogravimetric analysis (TGA) was performed to evaluate the thermal stability of BiOCl/CNC. As shown in [Fig. S2](#), BiOCl/CNC has high thermal stability below 240 °C

Then the chemical states of the elements in the samples were analyzed by X-ray photoelectron spectroscopy (XPS). The binding energy of C 1s detected at 288.7 eV, 286.5 eV and 284.8 eV were attributed to C = O, O—C—O and C—OH, respectively, indicating that the carbon comes from cellulose ([Fig. S3a](#)) ([Du et al., 2019](#)). Obviously, the carbon content of BiOCl/CNC is greater than that of BiOCl, indicating that their combination is successful. [Fig. S3b](#) shows the binding energy values of Bi  $4f_{7/2}$  and Bi  $4f_{5/2}$  are observed at 164.5 eV and 159.2 eV, which ascribing to the  $\text{Bi}^{3+}$  in BiOCl ([Asadzadeh-Khaneghah et al., 2019](#); [Liang et al., 2020](#); [Jiang et al., 2022](#)). It should be noted that the interaction between BiOCl and CNC may result in the peak of BiOCl/CNC to be higher than that of BiOCl ([Ma et al., 2018](#)). As shown in [Fig. S3c](#), the peaks at 199.5 eV and 197.9 eV in BiOCl, which are well ascribed to Cl  $2p_{1/2}$  and Cl  $2p_{3/2}$ , respectively. Interestingly, two peaks become to 199.7 eV and 198.1 eV in BiOCl/CNC, which due to the tighter combination of  $\text{Cl}^-$  and BiOCl in the material ([Gao et al., 2019](#)). As depicted in [Fig. 2a](#), three distinct prominent peak peaks at 533.3 eV, 531.9 eV and 529.9 eV, which correspond to chemisorbed oxygen, oxygen vacancy and lattice oxygen, respectively ([Song et al., 2017](#)). Obviously, the oxygen vacancy peak shifted to high binding energy to 532.2 eV in BiOCl/CNC attributed to the interaction



**Scheme 1** Schematic illustration of the growth mechanism of BiOCl/CNC.

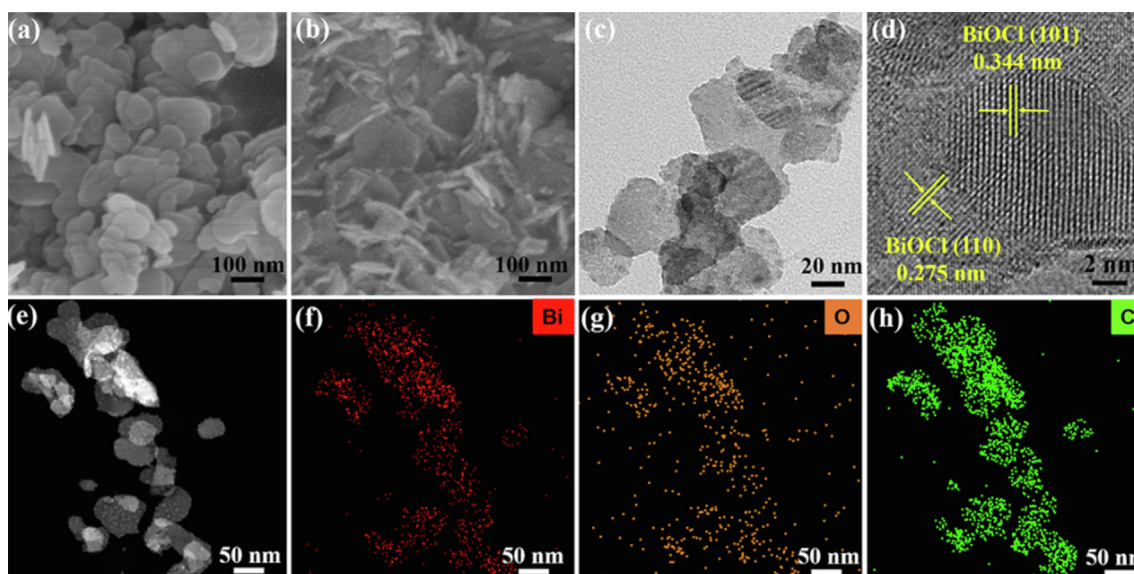


**Fig. 1** SEM images of (a) BiOCl, (b) BiOCl/CNC, TEM images of (c) BiOCl/CNC, HRTEM images of (d) BiOCl/CNC; Element mapping of Bi, O and Cl for BiOCl/CNC composite (e-h).

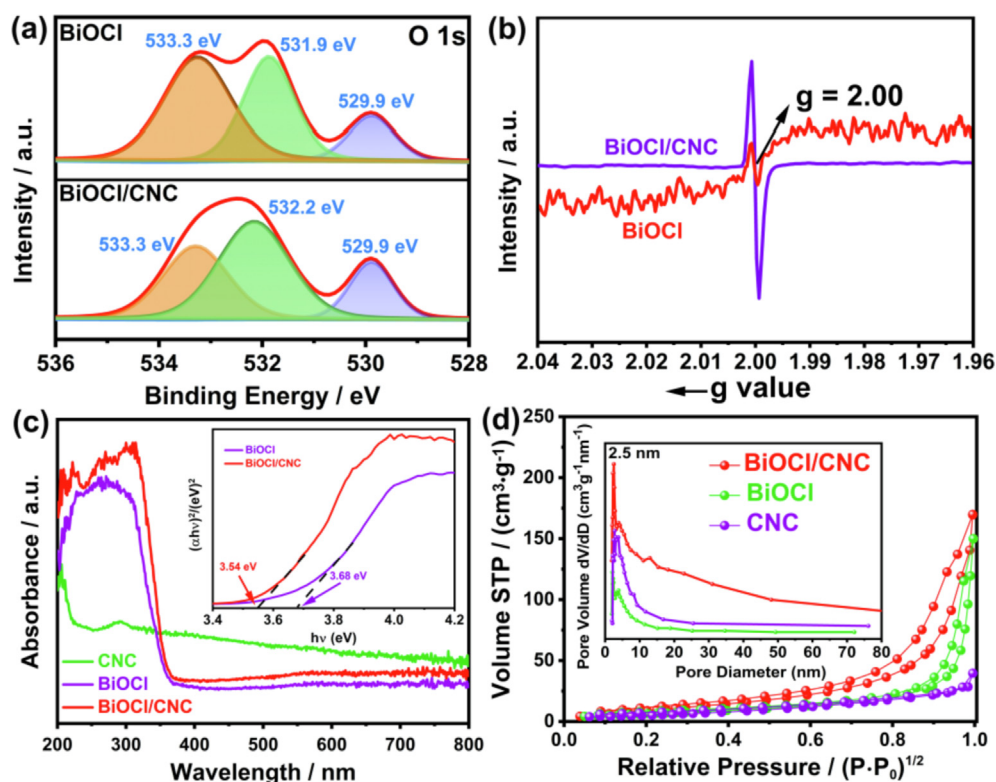


**Fig. 2** (a) XPS spectra in the O1s region of BiOCl and BiOCl/CNC. (b) ESR spectra of BiOCl and BiOCl/CNC. (c) UV-vis absorption spectra of the samples (inset: plot of bandgap). (d) Nitrogen adsorption-desorption isotherms (inset: pore size distribution).

between BiOCl and CNC (Wang et al., 2013). In addition, it can be seen the content of vacant oxygen on the surface increases significantly, which may be due to the strong interfacial hydrogen bonds between CNC and BiOCl weakening the surface Bi-O bonds (Li et al., 2020). In order to further con-

firm the existence of oxygen vacancy in BiOCl/CNC, we characterized it by electron spin-resonance spectroscopy (ESR) and the signal of BiOCl and BiOCl/CNC at  $g = 2.00$ , which is confirmed as oxygen vacancy (Fig. 2b) (Wu et al., 2021). Notably, the intensity of ESR signal for BiOCl/CNC is greater than that

of BiOCl, indicating that BiOCl/CNC has more oxygen vacancies, which is conducive to the improvement of photocatalytic performance (Ma et al., 2017). And UV–vis absorption spectrum shows that BiOCl/CNC has stronger visible light (400–800 nm) absorption than BiOCl, which is due to the increase of oxygen vacancies (Fig. 2c) (Li et al., 2018). As shown in the inset, the band gap energy of BiOCl and BiOCl/CNC were calculated as 3.68 and 3.54 eV, respectively (Kong et al., 2021). In addition, the specific surface areas and pore structure of the photocatalysts were analyzed through the study of N<sub>2</sub> adsorption/desorption. Test results indicate there is a significant hysteresis loop belonging to H-III of type IV, suggesting the presence of mesopores structure, which allows small organic molecules to pass through (Fig. 2d) (Hou et al., 2018). The BET surface area of BiOCl and BiOCl/CNC were calculated to be 23.46 m<sup>2</sup>g<sup>-1</sup> and 53.79 m<sup>2</sup>g<sup>-1</sup>, respectively, which is evident that the addition of CNC increases the surface area compared to BiOCl. Generally speaking, higher surface area can make the photogenerated charge transfer faster and can absorb more active substances and reactants to improve the reaction efficiency. The pore size distribution of the samples falls in the range of 2–8 nm.

Furthermore, the transient photocurrent response, electrochemical impedance spectroscopy (EIS) and the photoluminescence (PL) were applied to examine the photogenerated electron migration barrier and separation efficiency of photogenerated charge carriers. As shown in Fig. S4a, BiOCl/CNC showed the highest photocurrent density, which reflects the most effective charge separation. CNC showed a flat curve due to the balanced rate of charge diffusion within the CNC and rate of reaction at the interface between CNC and electrolyte. BiOCl showed a charging curvature photocurrent, which means that the rate of charge transfer with the BiOCl was higher than the rate of the surface reaction. However, BiOCl/CNC presented a blocking curvature, because the rate of surface reaction is limiting the photocurrent.

Fig. S4b depicts the EIS Nyquist plots of BiOCl/CNC, BiOCl and CNC, obviously, BiOCl/CNC has the smallest arc radius in comparison with BiOCl and CNC, which suggests that the combination of CNC and BiOCl can improve the efficiency of charge separation and transfer (Wang et al., 2020). Consistence with EIS, the PL spectrum of BiOCl/CNC in Fig. S4c illustrates the weaker intensity than BiOCl, implying lower recombination rate of electrons-holes and higher photoactivity of the photocatalyst (Li et al., 2021; Wang et al., 2013). Based on the transient photocurrent response, EIS and PL results, the composite material may exhibit better photocatalytic performance than BiOCl due to the strong interaction between BiOCl and CNC.

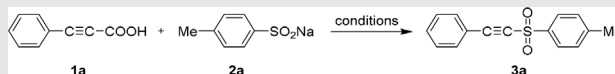
### 3.2. Photocatalytic performance test of BiOCl/CNC to sulfonylation of arylacetylenic acids with sodium arylsulfonates

Table 1 lists the exploratory experimental results of arylacetylene sulfone prepared by sulfonation of arylacetylene acid and sodium sulfite under different conditions. Initially, 3-phenylpropionic acid (**1a**, 0.5 mmol) was treated with sodium *p*-toluenesulfonate (**2a**, 1.0 mmol), BiOCl/CNC (20 mg) in THF (4.5 mL) and the solution was stirred for 20 h under white LED light in the presence of oxygen, however, target compound was not synthesized (Table 1, entry 1). Interestingly,

the desired compound was obtained in 73% yield when iodine (0.25 eq.) was added as an initiator (Table 1, entry 2). If iodine was added to the reaction without BiOCl/CNC, the yield was significantly reduced to 44% (Table 1, entry 3), indicating the synergistic effect of BiOCl/CNC and iodine. And the yield of product will drastically decrease when exposed to air, even in the presence of iodine and BiOCl/CNC (Table 1, entry 4), which indicates that oxygen is one of the essential factors to achieve this reaction. Subsequently, the reaction was carried without visible light, only 10% of the product was obtained, indicating the light source is also the key factor (Table 1, entry 5). The yield increased from 73% to 89% when the dosage of iodine was added to 0.5 eq., and further increase of the amount of iodine did not give rise to a significantly improvement in yield (Table 1, entries 6 and 7). As a result, the appropriate amount of iodine (0.5 eq.) was conducive to the reaction. On the basis, the yield of the product decreases significantly without BiOCl/CNC in the reaction (Table 1, entry 8), which result further confirming the necessity of the BiOCl/CNC. In summary, iodine, BiOCl/CNC, oxygen and LED light are all indispensable to achieve the product efficiently. When the photocatalyst was replaced by pure BiOCl and CNC, the yields of the target product were not optimistic (Table 1, entries 9 and 10).

Subsequently, the reaction efficiency was not further improved after a series of adjustment of the amount of BiOCl/CNC (Table 1, entries 11 and 12). If the reaction time was shortened or prolonged to 16 h or 24 h, the yield became 60% and 88%, respectively (Table 1, entries 13 and 14). The influence of different color light sources on the reaction was explored, and the result showed that white LED light was the best light source (Table 1, entries 6, 15–17), and various solvents were screened (Table 1, entries 18–25). Eventually, THF was considered to be an optimum solvent for increasing the yield of **3a** (89% yield), and the optimized reaction conditions was determined in entry 6 of Table 1. According to the above series of conditional experiments, the optimal reaction conditions are as follows: in the presence of 20 mg of BiOCl/CNC and 0.5 equivalent of iodine, 30 W white LED lamp and THF were used as the light source and solvent, the reaction was carried out at rt for 20 h.

Under the optimal reaction conditions, the generality and functional group compatibility of the transformation were tested, and the results are summarized in Table 2 and Table 3. First of all, the scope of the various arylacetylenic acids with **2a** was investigated (Table 2). Generally speaking, arylacetylenic acids contain a broad range of electron donating groups could successfully delivered the desired compounds **3a**–**3d** in satisfactory yields (75%–96%). However, when the electron donating groups on arylacetylene acid were located in ortho and meta positions (**3e** and **3f**), the yield of the reaction decreased, suggesting that the steric hindrance has a greater impact on the reaction results than the electron effect. If the arylacetylenic acid contains a strong electron withdrawing group (*p*-CF<sub>3</sub>), the conversion yield of **3g** was significantly reduced (36%). In addition, thiophen-2-ylpropionic acid and naphthalene-2-ylpropionic acid also possess outstanding adaptability. The yields of **3h** and **3i** were 54% and 87%, respectively. Subsequently, the sulfonation reaction of **1a** with a series of sodium sulfonates were tried under the optimum conditions, which was summarized in Table 3. Sodium sulfonates containing electron donating group or electron withdrawing

**Table 1** Photocatalytic sulfonation of arylacetylenic acids with sodium arylsulfonates.

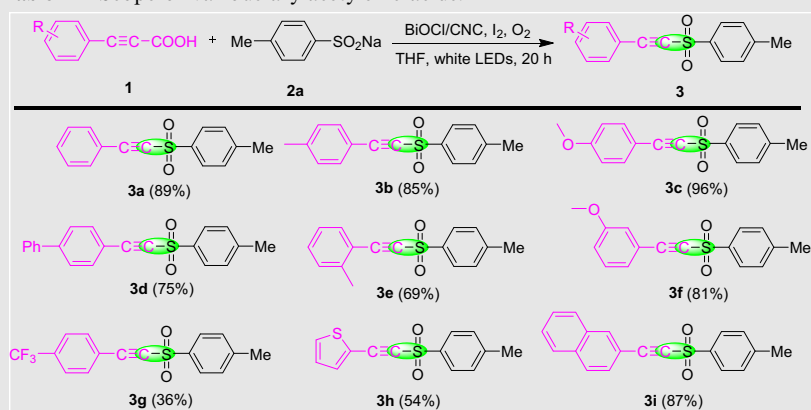
Entry	I <sub>2</sub> (eq.)	BiOCl/CNC	Solvent	Light	Yield <sup>a</sup> (%)
1	—	20 mg	THF	On	—
2	0.25	20 mg	THF	On	73
3	0.25	—	THF	On	44
4 <sup>b</sup>	0.25	20 mg	THF	On	26
5	0.25	20 mg	THF	Dark	10
6	0.5	20 mg	THF	On	89
7	1.0	20 mg	THF	On	87
8	0.5	—	THF	On	52
9 <sup>c</sup>	0.5	20 mg	THF	On	68
10 <sup>d</sup>	0.5	20 mg	THF	On	65
11	0.5	15 mg	THF	On	72
12	0.5	25 mg	THF	On	88
13 <sup>e</sup>	0.5	20 mg	THF	On	60
14 <sup>f</sup>	0.5	20 mg	THF	On	88
15	0.5	20 mg	THF	Red	17
16	0.5	20 mg	THF	Blue	80
17	0.5	20 mg	THF	Green	25
18	0.5	20 mg	CH <sub>3</sub> CN	On	40
19	0.5	20 mg	EtOH	On	37
20	0.5	20 mg	DMAc	On	32
21	0.5	20 mg	DMF	On	23
22	0.5	20 mg	DMSO	On	trace
23	0.5	20 mg	DCE	On	—
24	0.5	20 mg	1,4-Dioxane	On	trace
25	0.5	20 mg	Toluene	On	trace

<sup>a</sup> Isolated yields after column chromatography.

<sup>b</sup> Reaction was performed in air.

<sup>c,d</sup> BiOCl and CNC were used respectively.

<sup>e,f</sup> Reaction for 16 h and 24 h respectively.

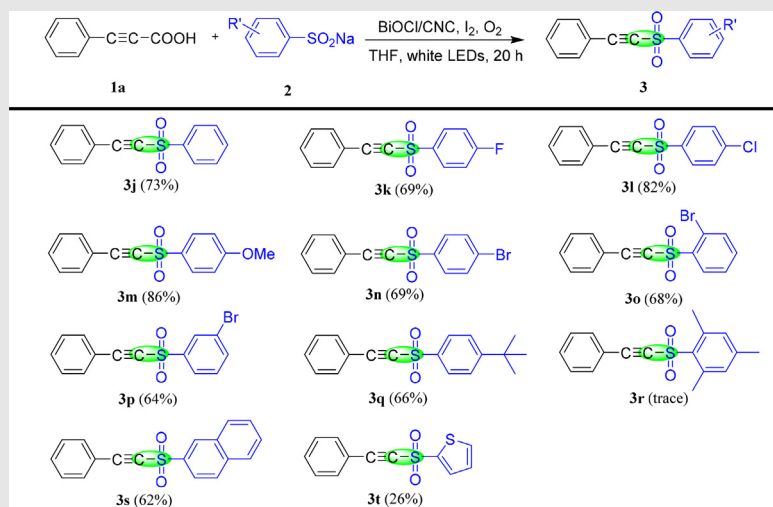
**Table 2** Scope of various arylacetylenic acids.<sup>a,b</sup>

<sup>a</sup> Conditions: **1** (0.5 mmol), **2a** (1.0 mmol), I<sub>2</sub> (0.5 eq.), BiOCl/CNC (20 mg) in THF (4.5 mL), O<sub>2</sub>, 30 W white LED, rt, 20 h.

<sup>b</sup> Isolated yields by column chromatography based on **1**.

group could not significantly affect the reaction results, and all could be obtained products **3j-3q** in satisfactory yields (64%–86%). Notably, it was found that the spatial effect of

substituents on sodium sulfonate was weaker than that of arylacetylene acid by analyzing the reaction results of **3n**, **3o** and **3p**. However, if 1,3,5-trimethyl-2-(2-phenyl-ethynylsulfonyl)-

**Table 3** Scope of various sodium arylsulfonates.<sup>a,b</sup>

<sup>a</sup> Conditions: **1a** (0.5 mmol), **2** (1.0 mmol), I<sub>2</sub> (0.5 eq.), BiOCl/CNC (20 mg) in THF (4.5 mL), O<sub>2</sub>, 30 W white LED, rt, 20 h.

<sup>b</sup> Isolated yields by column chromatography based on **1a**.

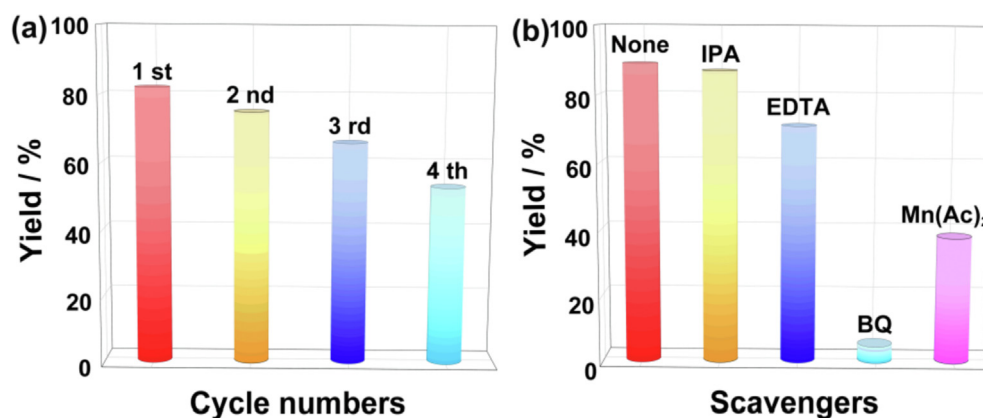


**Fig. 3** (a) The cycling experiment of BiOCl/CNC. (b) Radical trapping experiment of sulfonylation of arylacetylenic acid with sodium arylsulfinate.

benzene is used in the reaction, only trace product **3r** could be detected by TLC due to the large space hindrance effect of substituents. Moreover, sodium naphthalene-2-sulfinate and sodium thiophene-2-sulfinate were also provide the desired product **3s** and **3t** in 62% and 26% yields, respectively.

To evaluate the recyclability of the BiOCl/CNC photocatalyst, a recycling experiment is shown in Fig. 3a. The used BiOCl/CNC was washed with water and ethanol in turn, after natural drying, it can be directly used for the next round of reaction without adding new catalyst. After four cycles of photocatalytic experiments, the yield by recycled BiOCl/CNC could still reach 53%, indicating a good recycling performance. The XRD (Fig. S5a) and IR (Fig. S5b) results of the recovered BiOCl/CNC showed that the diffraction and vibration peaks were not significantly different from those of the fresh BiOCl/CNC, indicating that the BiOCl / CNC had excellent photostability. In addition, the morphology of cycled sample maintained a complete lamellar structure by the TEM

characterization (Fig. S6a). Elemental analysis also showed uniform distribution of elements on the cycled sample (Fig. S6b-e). All these results can demonstrate the photostability of the composites. Thus, the decrease of catalyst activity during recycling can be speculated to the unavoidable loss of catalyst during recovery.

### 3.3. Photocatalytic mechanism study of BiOCl/CNC to sulfonylation of arylacetylenic acids with sodium arylsulfonates

In order to explore the predominant active species involved in the process of photocatalytic reduction, isopropyl alcohol (IPA), EDTA-2Na, benzoquinone (BQ) and Mn(Ac)<sub>2</sub> were applied as the sacrificial agents for hydroxyl radical ( $\cdot\text{OH}$ ), holes ( $h^+$ ), superoxide radical ( $\text{O}_2^{\cdot-}$ ) and photogenerated electrons ( $e^-$ ), respectively. In addition to adding scavengers, the capture tests were carried out under the same conditions as the photocatalytic test. Obviously, the introduction of BQ



### CRedit authorship contribution statement

**Xiaoxia Wang:** Conceptualization, Methodology, Data curation, Visualization, Writing – original draft. **Xueting Li:** Investigation, Formal analysis. **Baoqiang Tian:** Investigation. **He Xiao:** Funding acquisition. **Wenwen Chen:** Methodology, Writing – review & editing. **Haishun Wu:** Investigation. **Jianfeng Jia:** Methodology, Supervision, Writing – review & editing.

### Declaration of Competing Interest

The authors declare that they have no known competing financial interests or personal relationships that could have appeared to influence the work reported in this paper.

### Acknowledgments

This work was supported by the National Natural Science Foundation of China (No. 21571119), the Applied Basic Research Project of Shanxi Province (No. 201901D211393), the graduate Education Innovation Project of Shanxi Province (No. 2020BY081) and the graduate Education Innovation Project of Shanxi Normal University (2019XBY013 and 2019XBY016).

### Appendix A. Supplementary data

Supplementary data to this article can be found online at <https://doi.org/10.1016/j.arabjc.2022.103708>.

### References

- Asadzadeh-Khaneghah, S., Habibi-Yangjeh, A., Yubuta, K., 2019. Novel g-C<sub>3</sub>N<sub>4</sub> nanosheets/CDs/BiOCl photocatalysts with exceptional activity under visible light. *J. Am. Ceram. Soc.* 102, 1435–1453. <https://doi.org/10.1111/jace.15959>.
- Chen, P., Zhu, C., Zhu, R., Wu, W., Jiang, H., 2017. MnO<sub>2</sub>-promoted oxidative radical sulfonylation of haloalkynes with sulfonyl hydrazides: C(sp)-S bond formation towards alkynyl sulfones. *Chem. Asian J.* 12, 1875–1878. <https://doi.org/10.1002/asia.201700550>.
- Du, M., Du, Y., Feng, Y., Li, Z., Wang, J., Jiang, N., Liu, Y., 2019. Advanced photocatalytic performance of novel BiOBr/BiOI/cellulose composites for the removal of organic pollutant. *Cellulose* 26, 5543–5557. <https://doi.org/10.1007/s10570-019-02474-1>.
- Du, M., Du, Y., Feng, Y., Yang, K., Lv, X., Jiang, N., Liu, Y., 2018. Facile preparation of BiOBr/cellulose composites by in situ synthesis and its enhanced photocatalytic activity under visible-light. *Carbohydr. Polym.* 195, 393–400. <https://doi.org/10.1016/j.carbpol.2018.04.092>.
- Elfeky, A.S., Salem, S.S., Elzaref, A.S., Owda, M.E., Eladawy, H.A., Saeed, A.M., Awad, M.A., Abou-Zeid, R.E., Fouda, A., 2020. Multifunctional cellulose nanocrystal /metal oxide hybrid, photo-degradation, antibacterial and larvicidal activities. *Carbohydr. Polym.* 230, 115711. <https://doi.org/10.1016/j.carbpol.2019.115711>.
- Fava, E., Millet, A., Nakajima, M., Loescher, S., Rueping, M., 2016. Reductive umpolung of carbonyl derivatives with visible-light photoredox catalysis: direct access to vicinal diamines and amino alcohols via  $\alpha$ -amino radicals and ketyl radicals. *Angew. Chem. Int. Ed.* 55, 6776–6779. <https://doi.org/10.1002/anie.201511235>.
- Gao, X., Tang, G., Peng, W., Guo, Q., Luo, Y., 2019. Surprise in the phosphate modification of BiOCl with oxygen vacancy: In situ construction of hierarchical Z-scheme BiOCl-OV-BiPO<sub>4</sub> photocatalyst for the degradation of carbamazepine. *Chem. Eng. J.* 360, 1320–1329. <https://doi.org/10.1016/j.cej.2018.10.216>.
- Gao, X., Zhang, X., Wang, Y., Peng, S., Yue, B., Fan, C., 2015. Rapid synthesis of hierarchical BiOCl microspheres for efficient photocatalytic degradation of carbamazepine under simulated solar irradiation. *Chem. Eng. J.* 263, 419–426. <https://doi.org/10.1016/j.cej.2014.10.110>.
- Gao, X., Peng, W., Tang, G., Guo, Q., Luo, Y., 2018. Highly efficient and visible-light-driven BiOCl for photocatalytic degradation of carbamazepine. *J. Alloys Compd.* 757, 455–465. <https://doi.org/10.1016/j.jallcom.2018.05.081>.
- Gao, X., Guo, Q., Tang, G., Zhu, W., Yang, X., Luo, Y., 2020. TBAOH assisted synthesis of ultrathin BiOCl nanosheets with enhanced charge separation efficiency for superior photocatalytic activity in carbamazepine degradation. *J. Colloid Interface Sci.* 570, 242–250. <https://doi.org/10.1016/j.jcis.2020.02.065>.
- Gao, X., Gong, C., Wang, X., Zhu, W., Luo, Y., 2021. Facile synthesis of cobalt doped BiOCl ultrathin nanosheets as superior photocatalyst for degradation of carbamazepine under visible light. *J. Solid State Chem.* 298, . <https://doi.org/10.1016/j.jssc.2021.122131>.
- Guerrero, M., Altube, A., Garcia-Lecina, E., Rossinyol, E., Baro, M. D., Pellicer, E., Sort, J., 2014. Facile in situ synthesis of BiOCl nanoplates stacked to highly porous TiO<sub>2</sub>: a synergistic combination for environmental remediation. *ACS Appl. Mater. Interfaces* 6, 13994–14000. <https://doi.org/10.1021/am5033549>.
- Hamad, W.Y., 2018. Cellulose nanocrystals properties, production and applications, in: applications of cellulose nanocrystals. *MRS Bulletin*, 155. <https://doi.org/10.1557/mrs.2018.139>.
- Han, A., Sun, J., Zhang, H., Chuah, G.-K., Jaenicke, S., 2019. Visible light induced selective aerobic formation of N-benzylidene benzylamine over 2-aminoterephthalic acid sensitized {110}-faceted BiOCl nanosheets. *ChemCatChem* 11, 6425–6430. <https://doi.org/10.1002/cctc.201901562>.
- Han, Q., 2021. Advances in preparation methods of bismuth-based photocatalysts. *Chem. Eng. J.* 414. <https://doi.org/10.1016/j.cej.2020.127877>.
- Hojamberdiev, M., Kadirova, Z.C., Zahedi, E., Onna, D., Claudia Marchi, M., Zhu, G., Matsushita, N., Hasegawa, M., Aldabe Bilmes, S., Okada, K., 2020. Tuning the morphological structure, light absorption, and photocatalytic activity of Bi<sub>2</sub>WO<sub>6</sub> and Bi<sub>2</sub>WO<sub>6</sub>-BiOCl through cerium doping. *Arab. J. Chem.* 13, 2844–2857. <https://doi.org/10.1016/j.arabjc.2018.07.014>.
- Hou, X., Xue, S., Liu, M., Shang, X., Fu, Y., He, D., 2018. Hollow irregular octahedra-like NiCo<sub>2</sub>O<sub>4</sub> cages composed of mesoporous nanosheets as a superior anode material for lithium-ion batteries. *Chem. Eng. J.* 350, 29–36. <https://doi.org/10.1016/j.cej.2018.05.164>.
- Hu, Z., Meng, Q., Liu, R., Fu, S., Lucia, L.A., 2017. Physical study of the primary and secondary photothermal events in gold/cellulose nanocrystals (AuNP/CNC) nanocomposites embedded in PVA matrices. *ACS Sustain. Chem. Eng.* 5, 1601–1609. <https://doi.org/10.1021/acssuschemeng.6b02380>.
- Huang, Y., Zhao, P., Miao, H., Shao, S., Wang, L., Chen, Y., Jia, C., Xia, J., 2021. Organic-inorganic TCP/P/BiOCl hybrids with accelerated interfacial charge separation for boosted photocatalytic performance. *Colloids Surf. A Physicochem. Eng. Asp.* 616, . <https://doi.org/10.1016/j.colsurfa.2021.126367>.
- Jia, Z., Lv, R., Guo, L., Zhang, J., Li, R., Liu, J., Fan, C., 2021. Rapid degradation of ciprofloxacin over BiOCl: Insight into the molecular structure transformation and antibacterial activity elimination. *Sep. Purif. Technol.* 257, . <https://doi.org/10.1016/j.seppur.2020.117872>.
- Jiang, X., Kong, D., Luo, B., Wang, M., Zhang, D., Pu, X., 2022. Preparation of magnetically retrievable flower-like AgBr/BiOBr/NiFe<sub>2</sub>O<sub>4</sub> direct Z-scheme heterojunction photocatalyst with enhanced visible-light photoactivity. *Colloids Surf. A Physicochem. Eng. Asp.* 633. <https://doi.org/10.1016/j.colsurfa.2021.127880>.

- Kamel, S., Khattab, T.A., 2021. Recent advances in cellulose supported metal nanoparticles as green and sustainable catalysis for organic synthesis. *Cellulose* 28, 4545–4574. <https://doi.org/10.1007/s10570-021-03839-1>.
- Kong, D., Fan, H., Yin, D., Zhang, D., Pu, X., Yao, S., Su, C., 2021. AgFeO<sub>2</sub> nanoparticle/ZnIn<sub>2</sub>S<sub>4</sub> microsphere p–n heterojunctions with hierarchical nanostructures for efficient visible-light-driven H<sub>2</sub> evolution. *ACS Sustain. Chem. Eng.* 9, 2673–2683. <https://doi.org/10.1021/acssuschemeng.0c07638>.
- Li, H., Chen, S., Shang, H., Wang, X., Yang, Z., Ai, Z., Zhang, L., 2020. Surface hydrogen bond network spatially confined BiOCl oxygen vacancy for photocatalysis. *Sci. Bull.* 65, 1916–1923. <https://doi.org/10.1016/j.scib.2020.06.013>.
- Li, H., Li, J., Ai, Z., Jia, F., Zhang, L., 2018. Oxygen Vacancy-Mediated Photocatalysis of BiOCl: Reactivity, Selectivity, and Perspectives. *Angew. Chem. Int. Ed.* 57, 122–138. <https://doi.org/10.1002/anie.201705628>.
- Li, Y.-L., Liu, Y., Mu, H.-Y., Liu, R.-H., Hao, Y.-J., Wang, X.-J., Hildebrandt, D., Liu, X., Li, F.-T., 2021. The simultaneous adsorption, activation and in situ reduction of carbon dioxide over Au-loading BiOCl with rich oxygen vacancies. *Nanoscale* 13, 2585–2592. <https://doi.org/10.1039/D0NR08314C>.
- Liang, S., Zhang, D., Yao, X., Han, R., Zhang, Q., Jin, C., Pu, X., Geng, Y., 2020. Deposition-precipitation synthesis of Yb<sup>3+</sup>/Er<sup>3+</sup> co-doped BiOBr/AgBr heterojunction photocatalysts with enhanced photocatalytic activity under Vis/NIR light irradiation. *Sep. Purif. Technol.* 238, <https://doi.org/10.1016/j.seppur.2019.116450> 116450.
- Liu, Y., Xu, J., Chen, M., 2021. Synthesis of direct Z-Scheme Bi<sub>3</sub>NbO<sub>7</sub>/BiOCl photocatalysts with enhanced activity for CIP degradation and Cr(VI) reduction under visible light irradiation. *Sep. Purif. Technol.* 276, <https://doi.org/10.1016/j.seppur.2021.119255> 119255.
- Llamas, T., Arrayás, R.G., Carretero, J.C., 2006. Catalytic enantioselective 1,3-dipolar cycloaddition of azomethine ylides with vinyl sulfones. *Org. Lett.* 8, 1795–1798. <https://doi.org/10.1021/ol060314c>.
- Ma, D., Zhong, J., Li, J., Wang, L., Peng, R., 2018. Enhanced photocatalytic activity of BiOCl by C<sub>70</sub> modification and mechanism insight. *Appl. Surf. Sci.* 443, 497–505. <https://doi.org/10.1016/j.apsusc.2018.03.018>.
- Ma, Z., Li, P., Ye, L., Zhou, Y., Su, F., Ding, C., Xie, H., Bai, Y., Wong, P.K., 2017. Oxygen vacancies induced exciton dissociation of flexible BiOCl nanosheets for effective photocatalytic CO<sub>2</sub> conversion. *J. Mater. Chem. A* 5, 24995–25004. <https://doi.org/10.1039/C7TA08766G>.
- Mansor, E.S., Geioushy, R.A., Fouad, O.A., 2021. PANI/BiOCl nanocomposite induced efficient visible-light photocatalytic activity. *J. Mater. Sci. Mater. Electron.* <https://doi.org/10.1007/s10854-020-04966-4>.
- Meadows, D.C., Gervay-Hague, J., 2006. Vinyl sulfones: synthetic preparations and medicinal chemistry applications. *Med. Res. Rev.* 26, 793–814. <https://doi.org/10.1002/med.20074>.
- Meesin, J., Katrun, P., Paresecharoen, C., Pohmakotr, M., Reutrakul, V., Soorukram, D., Kuhakarn, C., 2016. Iodine-catalyzed sulfonylation of arylacetylenic acids and arylacetylenes with sodium sulfonates: synthesis of arylacetylenic sulfones. *J. Org. Chem.* 81, 2744–2752. <https://doi.org/10.1021/acs.joc.5b02810>.
- Monga, D., Basu, S., 2021. Single-crystalline 2D BiOCl nanorods decorated with 2D MoS<sub>2</sub> nanosheets for visible light-driven photocatalytic detoxification of organic and inorganic pollutants. *FlatChem* 28, <https://doi.org/10.1016/j.flatc.2021.100267> 100267.
- Ng, L.Y., Wong, T.J., Ng, C.Y., Amelia, C.K.M., 2021. A review on cellulose nanocrystals production and characterization methods from *Elaeis guineensis* empty fruit bunches. *Arab. J. Chem.* 14, <https://doi.org/10.1016/j.arabjc.2021.103339> 103319.
- Riddell, N., Tam, W., 2006. Ruthenium-catalyzed [2+2] cycloadditions of alkynyl sulfides and alkynyl sulfones. *J. Org. Chem.* 71, 1934–1937. <https://doi.org/10.1021/jo052295a>.
- Shi, C., Zhang, L., Bian, H., Shi, Z., Ma, J., Wang, Z., 2021. Construction of Ag–ZnO/cellulose nanocomposites via tunable cellulose size for improving photocatalytic performance. *J. Clean. Prod.* 288, <https://doi.org/10.1016/j.jclepro.2020.125089> 125089.
- Soleimani, F., Salehi, M., Gholizadeh, A., 2017. Hydrothermal synthesis, structural and catalytic studies of CuBi<sub>2</sub>O<sub>4</sub> nanoparticles. *J. Nanoanalysis.* 20, 585–593. <https://doi.org/10.22034/jna.2017.542053.1019>.
- Song, Z., Dong, X., Wang, N., Zhu, L., Luo, Z., Fang, J., Xiong, C., 2017. Efficient photocatalytic defluorination of perfluorooctanoic acid over BiOCl nanosheets via a hole direct oxidation mechanism. *Chem. Eng. J.* 317, 925–934. <https://doi.org/10.1016/j.cej.2017.02.126>.
- Sulzer-Mosse, S., Alexakis, A., Mareda, J., Bollot, G., Bernardinelli, G., Filinchuk, Y., 2009. Enantioselective organocatalytic conjugate addition of aldehydes to vinyl sulfones and vinyl phosphonates as challenging Michael acceptors. *Chem. Eur. J.* 15, 3204–3220. <https://doi.org/10.1002/chem.200801892>.
- Tian, C., Luo, S., She, J., Qing, Y., Yan, N., Wu, Y., Liu, Z., 2019. Cellulose nanofibrils enable flower-like BiOCl for high-performance photocatalysis under visible-light irradiation. *Appl. Surf. Sci.* 464, 606–615. <https://doi.org/10.1016/j.apsusc.2018.09.126>.
- Todoroki, H., Iwatsu, M., Urabe, D., Inoue, M., 2014. Total synthesis of (-)-4-hydroxyzinowol. *J. Org. Chem.* 79, 8835–8849. <https://doi.org/10.1021/jo501666x>.
- Wang, L., Wei, W., Yang, D., Cui, H., Yue, H., Wang, H., 2017. Direct cross-coupling of aryl alkynyl iodides with arylsulfonic acids leading to alkynyl sulfones under catalyst-free conditions. *Tetrahedron Lett.* 58, 4799–4802. <https://doi.org/10.1016/j.tetlet.2017.11.029.242>.
- Wang, X.-J., Wang, Q., Li, F.-T., Yang, W.-Y., Zhao, Y., Hao, Y.-J., Liu, S.-J., 2013. Novel BiOCl–C<sub>3</sub>N<sub>4</sub> heterojunction photocatalysts: In situ preparation via an ionic-liquid-assisted solvent-thermal route and their visible-light photocatalytic activities. *Chem. Eng. J.* 234, 361–371. <https://doi.org/10.1016/j.cej.2013.08.112>.
- Wang, X., Liu, X., Liu, G., Zhang, C., Liu, G., Xu, S., Cui, P., Li, D., 2019. Rapid synthesis of BiOCl graded microspheres with highly exposed (110) facets and oxygen vacancies at room temperature to enhance visible light photocatalytic activity. *Catal. Commun.* 130, 105769. <https://doi.org/10.1016/j.catcom.2019.105769>.
- Wang, Y., Wang, Q., Zhang, H., Wu, Y., Jia, Y., Jin, R., Gao, S., 2020. CTAB-assisted solvothermal construction of hierarchical Bi<sub>2</sub>MoO<sub>6</sub>/Bi<sub>5</sub>O<sub>7</sub>Br with improved photocatalytic performances. *Sep. Purif. Technol.* 242, 116775. <https://doi.org/10.1016/j.seppur.2020.116775>.
- Wu, S., Yu, X., Zhang, J., Zhang, Y., Zhu, Y., Zhu, M., 2021. Construction of BiOCl/CuBi<sub>2</sub>O<sub>4</sub> S-scheme heterojunction with oxygen vacancy for enhanced photocatalytic diclofenac degradation and nitric oxide removal. *Chem. Eng. J.* 411, 128555. <https://doi.org/10.1016/j.cej.2021.128555>.
- Wu, W., Song, Y., Bai, L., Chen, Z., Sun, H., Zhen, G., Zhan, R., Shen, Y., Qian, J., Yuan, Q., Sun, Z., 2020. Graphene oxide-BiOCl nanoparticle composites as catalysts for oxidation of volatile organic compounds in nonthermal plasmas. *ACS Appl. Nano Mater.* 3, 9363–9374. <https://doi.org/10.1021/acsnm.0c01994>.
- Xu, S., Zhou, P., Zhang, Z., Yang, C., Zhang, B., Deng, K., Bottle, S., Zhu, H., 2017. Selective oxidation of 5-hydroxymethylfurfural to 2,5-furandicarboxylic acid using O<sub>2</sub> and a photocatalyst of Co-thioporphyrazine bonded to g-C<sub>3</sub>N<sub>4</sub>. *J. Am. Chem. Soc.* 139, 14775–14782. <https://doi.org/10.1021/jacs.7b08861>.
- Yang, H., Carter, R.G., Zakharov, L.N., 2008. Enantioselective total synthesis of lycopodine. *J. Am. Chem. Soc.* 130, 9238–9239. <https://doi.org/10.1021/ja803613w>.

- Yang, X., Sun, S., Cui, J., Yang, M., Luo, Y., Liang, S., 2021. Synthesis, functional modifications, and diversified applications of hybrid BiOCl-based heterogeneous photocatalysts: a review. *Cryst. Growth Des.* 21, 6576–6618. <https://doi.org/10.1021/acs.cgd.1c00866>.
- Zhan, Y., Meng, Y., Li, W., Chen, Z., Yan, N., Li, Y., Teng, M., 2018. Magnetic recoverable MnFe<sub>2</sub>O<sub>4</sub>/cellulose nanocrystal composites as an efficient catalyst for decomposition of methylene blue. *Ind. Crops. Prod.* 122, 422–429. <https://doi.org/10.1016/j.indcrop.2018.06.043>.
- Zhang, D., Su, C., Yao, S., Li, H., Pu, X., Geng, Y., 2020. Facile in situ chemical transformation synthesis, boosted charge separation, and increased photocatalytic activity of BiPO<sub>4</sub>/BiOCl p-n heterojunction photocatalysts under simulated sunlight irradiation. *J. Phys. Chem. Solids* 147, 109630. <https://doi.org/10.1016/j.jpcs.2020.109630>.
- Zhang, X., Wang, X.-B., Wang, L.-W., Wang, W.-K., Long, L.-L., Li, W.-W., Yu, H.-Q., 2014. Synthesis of a highly efficient BiOCl single-crystal nanodisk photocatalyst with exposing 001 facets. *ACS Appl. Mater. Interfaces* 6, 7766–7772. <https://doi.org/10.1021/am5010392>.
- Zhao, P., Beaudry, C.M., 2014. Enantioselective and regioselective pyrone Diels-Alder reactions of vinyl sulfones: total synthesis of (+)-cavicularin. *Angew. Chem. Int. Ed.* 53, 10500–10503. <https://doi.org/10.1002/anie.201406621>.
- Zhong, Q., Zhao, Y., Sheng, S., Chen, J., 2020. Electrochemical decarboxylative sulfonylation of arylacetylenic acids with sodium arylsulfonates: Access to arylacetylenic sulfones. *Synth. Commun.* 50, 161–167. <https://doi.org/10.1080/00397911.2019.1686527>.
- Zhou, X., Yu, S., Qi, Z., Li, X., 2015. Rhodium(III)-catalyzed [3 + 2] annulative coupling between oximes and electron-deficient alkynes. *Sci. China. Chem.* 58, 1297–1301. <https://doi.org/10.1007/s11426-015-5408-8>.
- Zhu, Q., Cheng, L., Lu, Y., 2008. Asymmetric organocatalytic Michael addition of ketones to vinyl sulfone. *ChemComm*, 6315–6317. <https://doi.org/10.1039/b816307c>.